



A comparison of Structure from Motion Photogrammetry and the Traversing Micro Erosion Meter for measuring erosion on rock shore platforms.

5 Niamh D. Cullen¹, Ankit K. Verma¹ and Mary C. Bourke¹

¹Department of Geography, Trinity College Dublin, The University of Dublin, 2 College Green, Dublin 2, Ireland.

Correspondence to: Niamh D. Cullen (cullenni@tcd.ie)

Abstract

10 For decades researchers have used the Micro Erosion Meter and its successor the Traversing Micro Erosion Meter to measure microscale rates of vertical erosion (downwearing) on rock shore platforms. Difficulties with ‘upscaling’ of microscale field data in order to explain long term platform evolution have led to calls to introduce other methods which allow measurement of platform erosion at different scales. Structure from Motion Photogrammetry is fast emerging as a reliable, cost-effective tool for geomorphic change detection, providing a
15 valuable means for detecting micro to meso-scale geomorphic change over different terrain types. Here we present the results of an experiment where we test the efficacy of Structure from Motion Photogrammetry for measuring change on rock shore platforms due to different erosion processes (sweeping abrasion, scratching and percussion). Key to this approach is the development of the Coordinate Reference System used to reference and scale the models, and which can be easily deployed in the field. Experiments were carried out on three simulated platform
20 surfaces with low to high relative rugosity to assess the influence of surface roughness. We find that a Structure from Motion Photogrammetry can be used to reliably detect micro (sub mm) and meso (cm) scale erosion on shore platforms with a low Rugosity Index. As topographic complexity increases, the scale of detection is reduced. We also provide a detailed comparison of the two methods across a range of categories including cost, data collection, analysis and output. We find that Structure from Motion offers several advantages over the Micro
25 Erosion Meter, most notably the ability to detect and measure erosion of shore platforms at different scales.

Keywords

Shore platforms, Structure from Motion Photogrammetry, Traversing/Micro Erosion Metre, erosion.

1 Introduction

30 There are numerous methods employed for measuring natural rates of change on rock surfaces. For decades researchers were restricted to direct measurement of change relative to a datum, however this method has been



largely superseded by techniques which fall into two general categories; contact methods which utilise erosion meters, and non-contact methods such as Terrestrial Laser Scanning (TLS) and Structure from Motion (SfM) Photogrammetry (Moses et al., 2014). On rock shore platforms, the Micro Erosion Meter (MEM) and its successor the Transverse Micro Erosion Meter (TMEM) are the most frequently applied instruments for quantifying micro-scale erosion. However, SfM Photogrammetry is fast emerging as a valuable tool for detecting and quantifying geomorphic change across a range of scales and environments and represents a potential alternative to the MEM and TMEM for measuring erosion on shore platforms if a suitable level of resolution, accuracy and repeatability can be achieved. There is a large body of literature focussed on each of these methods (e.g. Carrivick et al., 2016; Gómez-Gutiérrez et al., 2014; Hanna, 1966; Kaiser et al., 2014; Smith et al., 2016; Snively, 2006; Stephenson and Finlayson, 2009; Stephenson et al., 2010; Stephenson and Kirk, 2001; Trenhaile, 2006; Trudgill, 1975; Trudgill et al., 1981; Westoby et al., 2012). A brief overview of the two methods is given below.

1.1 The Micro Erosion Meter and the Traversing Micro Erosion Meter

The MEM was developed and described by Hanna (1966) and High and Hanna (1970) as a tool for measuring relatively slow lowering rates of bedrock surfaces. Since its inception, the MEM and its modified successor, the TMEM (Trudgill et al., 1981) (hereafter T/MEM) have been used by numerous researchers to measure rates of surface lowering on shore platforms of varying lithologies. The spatial and temporal variability of measured erosion rates for shore platforms have allowed a more detailed understanding of processes operating on shore platform, contributing to the ongoing debate on the origin of shore platforms and the relative contributions of marine, biological and subaerial processes which drive their evolution (See Stephenson and Finlayson, 2009, for a more detailed review of the contribution of the T/MEM to rock coast research). The popularity of the T/MEM stems from the ability to detect sub-mm changes over short timescales (2 years) which, while comparative with the duration of many research projects, is also considered representative of longer-term (decadal) measurements (Stephenson et al., 2010). Add to this, the often cited low cost of construction and portability of the instrument and its popularity among rock coast researchers is easily understood.

Moses et al. (2014) outlined some limitations associated with the T/MEM. Authors studying erosion on (relatively soft) chalk platforms noted that the probe might cause erosion of the platform surface. This ‘probe erosion’ was also noted by Spate (1985). However, this does not constitute a problem where erosion rates are rapid (Foote et al., 2006; Swantesson et al., 2006). In addition, Moses et al., (2014) also noted that where rapid rates of erosion occur, this may result in the loosening or dislodgement of the bolts on which the T/MEM is placed on annual (Ellis, 1986; Andrews, 2000), or decadal timescales (Stephenson and Kirk, 1966). Trenhaile (2003) noted that although the T/MEM records small amounts of platform downwearing, it cannot record wave quarrying of larger blocks or loss of rock fragments due to frost riving.

Our use of the instrument has identified some additional limitations. First, the location of a T/MEM measurement station is limited to surfaces with low topographic complexity. This is an issue for shore platforms with highly variable meso and macro scale roughness and which only broadly conform to the Sunamura’s (1992) traditional Type A and Type B classification. Excluding these more complex platform morphologies significantly limits our ability to quantify rates and identify processes and styles of shore platform erosion across the complete spectrum



70 of platform morphologies. Second, while decades of measuring micro-scale erosion using the T/MEM have
provided valuable insights into rates and processes of downwearing on shore platforms, there are difficulties
associated with ‘up-scaling’ these field data to explain meso and macro-scale landform development (Warke and
McKinley, 2011). A recent study that reviewed 95 publications on shore platforms highlighted a concentration of
research on micro and macro scale studies. (Cullen and Bourke 2018), also noted by Stephenson and Naylor
75 (2011). In comparison, meso-scale processes have received less attention, although research at this scale has
increased significantly in the last two decades (Cullen and Bourke, 2018). Indeed, Stephenson et al. (2010)
advocated the introduction of new techniques which capture the full range of scales of erosion on shore platforms.
SfM Photogrammetry is one such technique that has this potential.

80 **1.2 Structure from Motion Photogrammetry**

Significant developments in digital photogrammetry techniques over the last decade have revolutionised the
collection of 3D topographic data in the geosciences. Traditional photogrammetry requires a knowledge of the
3D location and orientation of the camera and accurate 3D information of control points in the scene of interest.
While methods which allow the accurate calibration of non-metric cameras and reliable automation of the
85 photogrammetric process have enhanced the use of photogrammetry in the geosciences (e.g. Carbonneau et al.,
2004; Chandler, 1999; Chandler et al., 2002), it still requires expert understanding and practice (Carrivick et al.,
2016). In the last decade, there have been significant workflow advancements which have dramatically reduced
the expertise required. Structure from Motion (SfM) photogrammetry, uses a standard camera for collecting image
data of a three-dimensional (3D) landform.

90 Multiple overlapping images are taken from different spatial positions and used to reconstruct the 3D geometry
of the target. Unlike traditional photogrammetry, the SfM workflow does not require prior knowledge of the 3D
location, the camera orientation or 3D information on control points before reconstruction of scene geometry.
Rather, Scale Invariant Feature Detection (SIFT) (Lowe, 2004) is used to match points between images, and a
least square bundle adjustment algorithm is used to align images and produce a ‘sparse’ point cloud representing
95 the most prominent features in the images. A further development utilises Multi-View Stereo (SfM-MVS)
algorithms (e.g. Furukawa et al., 2010) to intensify the sparse cloud and merge the resulting 3D point cloud into
a single dense point-based model. This can then be used to generate a high-resolution ortho-photo, mesh or Digital
Elevation Model (DEM). Successive point clouds and DEMs of the same location or feature can be analysed
utilising widely available software (e.g. ArcMap, CloudCompare) for geomorphic change detection to quantify
100 erosion and deposition. A large amount of literature has been published on SfM, and the reader is referred to
Carrivick et al. (2016); Fonstad et al. (2013); Micheletti et al. (2015a, 2015b); Özyeşil et al. (2017); Smith et al.
(2016); Thoeni et al. (2014); Walkden and Hall (2005); Westoby et al. (2012), Verma and Bourke (for more
detailed discussions of SfM techniques and workflows.

The SfM-MVS workflow has been widely applied in the geosciences at varying scales of resolution from small
105 scale (mm - cm’s) scale studies of soil erosion to morphodynamic studies of beaches, coastal cliffs and braided
rivers (e.g. Balaguer-Puig et al., 2017; Brunier et al., 2016a; Brunier et al., 2016b; Javernick et al., 2014; Kaiser
et al., 2014; Lim et al., 2010). SfM-MVS offers several advantages over traditional surveying techniques,



specifically its relatively low cost and portability of required equipment, i.e. a camera, compared to that of TLS. In addition, the availability of free and relatively low cost commercial software, a semi-automated workflow and the decreasing cost of high-end desktop computers have resulted in the increasing application of this method in geomorphological research.

It is worth noting that the accuracy and resolution of SfM-MVS derived DEMs relies heavily on the quality of the images used and the accuracy of the coordinate reference system. For work on shore platforms, the accuracy of the DEM is limited by the accuracy of the Ground Control Points (GCPs) used. These are often determined using a Differential GPS (dGPS) or total stations which have reported accuracies of centimetres and millimetres respectively. However, a number of rock breakdown processes, such as granular disintegration (Viles, 2001) and features, such as weathering pits (Bourke et al., 2007; Thornbush, 2012; Viles, 2001) occur at cm to sub-mm scale.

Our work has three foci: First, to test the SfM-MVS for measuring micro-scale erosion on shore platforms. Second to determine the potential of SfM-MVS for meso-scale geomorphic change detection. Third, to provide a robust assessment and comparison of the two methods (T/MEM and SfM-MVS) for measuring erosion on shore platforms. Key to our approach is to adapt the local coordinate reference system (CRS), and SfM-MVS workflow developed by Verma and Bourke (Their system was developed to generate sub-mm scale DEMs of rock surfaces (<10 m²) in difficult to access terrains (e.g., cliffs and steep-sided impact crater walls). Their method can produce high resolution (sub-mm) DEMs with sub-mm accuracy. We advance this work through the design and manufacture of a field-hardy CRS which can be quickly deployed, repeatedly at the same site. Our approach will enable the application of SfM-MVS for geomorphic change detection on shore platforms at both the micro and meso scale.

In this paper we present the results of a series of experiments on simulated platform surfaces using our newly developed CRS.

2 Methods

2.1 A manufactured Coordinate Reference System for SfM-MVS

We have adapted the local coordinate reference system of (Verma and Bourke) which utilises a precisely measured equilateral triangle with a coded marker (downloaded from Agisoft Photoscan) attached at each vertex (Figure 1a and b). The x, y and z coordinates of each coded marker are calculated using trigonometry and serve as the GCPs for generating the DEMs in the SfM-MVS workflow. When used for a small surface area (≤ 6.76 m²), this method has been proved to produce high resolution (0.5 mm per pixel) DEMs with sub-mm accuracy (Verma and Bourke).

140

We mounted the coded markers onto a specifically designed stainless-steel platform (Fig. a and b). The platform consists of a 15 cm equilateral triangle with three square steel plates (4 cm x 4 cm x 0.5 cm) and a specially



machined leg. Each plate is engineered so that the centre of a plate is fixed precisely (± 0.01 mm) on one vertex of the triangular base. The centre of each plate is also permanently marked during manufacture so that the coded markers can be accurately placed. The base of the leg is machined to fit a stainless-steel square head bolt to a depth of 1.5 cm and is fixed at the centre of gravity on the underside of the triangular base plate.

In the field, the square headed bolt is fixed to the platform by drilling a hole and fixing the bolt with marine grade epoxy resin, making sure the bolt head is level. This is similar to the approach used to install T/MEM stations. When mounted onto the bolt, this design secures the base plate with the coordinate system in place with a high degree of relocation precision. This permits repeated measurements and the georeferencing of DEMs for high resolution change detection of field sites.

2.2 The experiments

The experiments were designed to capture different scales of erosion from granular scale abrasion of the platform surface to the removal of rock fragments. The accuracy of the SfM-MVS generated DEMs used to calculate DEMs of Difference (DoDs) for geomorphic change detection were assessed by means of horizontal and vertical checkpoints. We also investigated the influence of surface roughness on the accuracy of DEMs and resultant DoDs.

The experiment was set up outdoors on a level table (1.2 m x 0.6 m). Two scaled coded markers (0.25 m) and a series of 2.5 cm x 2.5 cm checkboard pattern, non-coded markers and eight, evenly spaced wooden blocks of known dimensions were fixed onto the table surface (Figure 1 C). These were used to calculate the horizontal and vertical error of the DEMs (as recommended by Verma and Bourke). Four simulated platform surface blocks were constructed using moulds, gypsum plaster. Stainless steel, square-headed bolts for mounting the CRS, as described above, were installed on each block. A digital inclinometer (Examobile Bubble Level for iPhone) was used to ensure the surface of the bolt was level. The surface of the experimental blocks were constructed to represent a range of micro to meso scale roughness that are observed in the field. These include low (B1), medium (B2) and high (B2) relative surface roughness (Figure 1 D-F). All blocks were sprayed with matte grey paint to allow easy identification of 'erosion' areas and provide additional visual validation of the models. A set of three 1 cm x 1 cm checkboard non-coded markers were fixed to each experimental block to serve as additional checkpoints for horizontal error. One block (B-con) was used as a control. The remaining three blocks (B1, B2 and B3) were used to carry out the experiment. Each block was placed at the centre of the table when acquiring images.

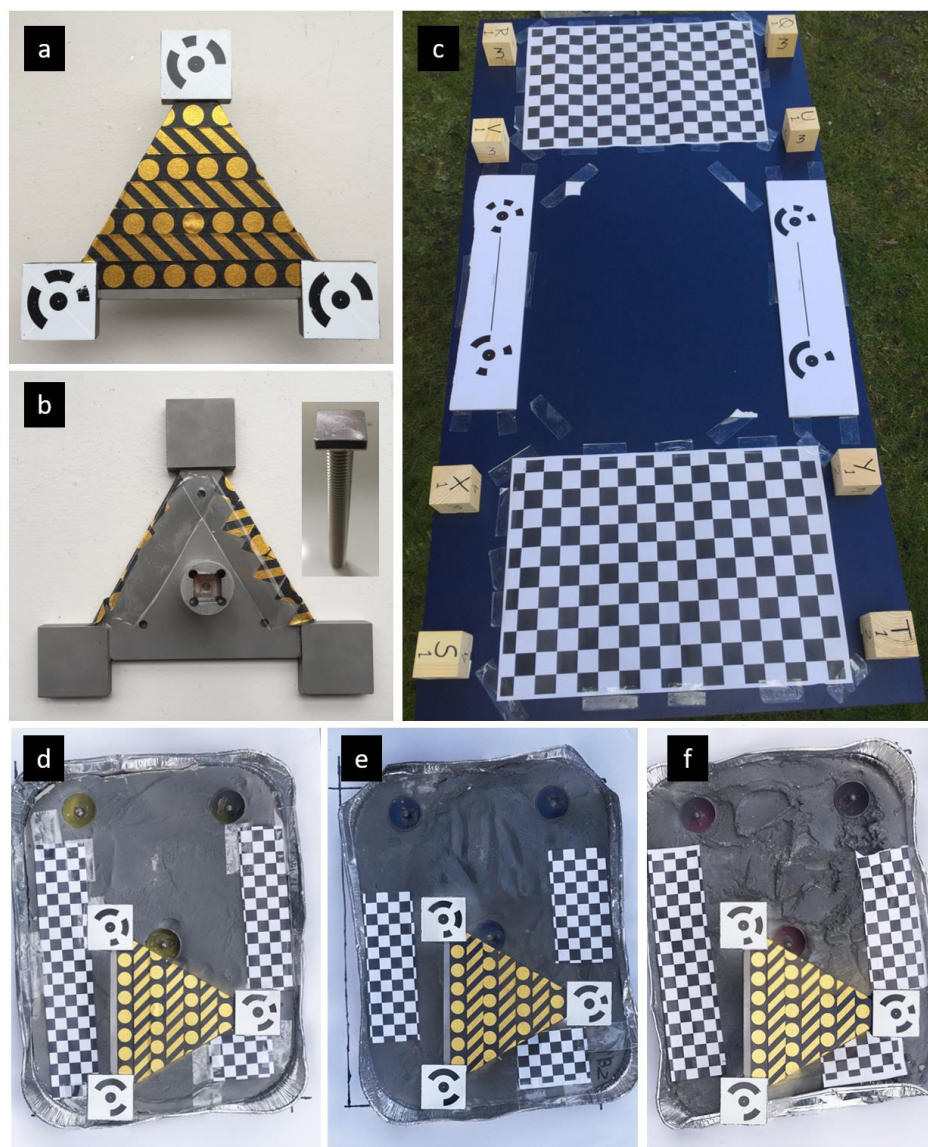


Figure 1. The experimental setup. a) The CRS top view and b) underside with the square headed bolt (inset) c) The experimental platform with markers and wooden blocks used to calculate the horizontal and vertical error. D, e, f) The simulated platform surface of experimental blocks B1, B2 and B3 designed with increasing roughness

175

2.3 Data collection

In order to replicate field conditions as closely as possible, all images of the experimental blocks were acquired outdoors during a single day. The CRS was placed on the pre-installed square head bolt, and orientation was noted. We used a Nikon D5500 with a variable zoom lens set up at 24 mm focal length.. Approximately 100 images of



180 each block were obtained. This number of images was required to capture the full extent of the table with the non-
coded markers and the wooden blocks used for the error analysis. We expect that 40-50 images would be
sufficient to generate a high-resolution DEM for a smaller area (e.g. <math><0.5\text{ m}^2</math>) in the field. In this study, ~70
images were acquired at a distance of ~1m from the experimental blocks and then a series (25-30 images) of close-
range shots at <math><0.5\text{ m}</math>. All three experimental blocks and the control block were imaged on the table prior to
185 simulating erosion on the blocks.

Recent work has demonstrated the potential efficacy of smaller-scale physical erosion processes on high energy
Atlantic rock platforms (Cullen and Bourke, 2018). However accurate quantification of these features has not
been possible. We therefore tested simulations of three known types of erosion: 1. Sweeping abrasion was
simulated by gently abrading the surface of all three blocks with a medium grit sandpaper. 2. Scratches were
190 simulated using a screwdriver 3. Impact percussion marks were simulated on one block using a hammer and
chisel.

The CRS was removed and replaced between each stage of data collection, as would be practice for carrying out
repeat surveys in the field. Images of the blocks were taken following simulated erosion as outlined above.

2.4 Repeatability

195 The utility of this approach for microscale change detection using the CRS developed for this study is contingent
on the exact replacement of the CRS during successive surveys in the field. To test the repeatability of this
approach, we used a control block to acquire images for DEM generation using the data collection and processing
procedure outlined above. At the end of the experiment, the CRS was replaced and a second series of images were
acquired for DEM generation for comparison. DEM accuracy and error propagation were calculated as described
200 below.

2.5 Data processing

2.5.1 Digital Elevation Models

All the images were acquired in raw format during the experiment. RAW images were converted to 14-bit
205 uncompressed tiff format with AdobeRGB colour space in Adobe Lightroom. We used Agisoft Photoscan (version
1.4.1). Image quality (Q) was assessed using the Estimate Image Quality tool in AgiSoft and images with Q values
<math><0.5</math> were removed. The CRS was used to scale and georeference the model. Baseline DEMs and orthophoto
mosaics for each block were generated and exported at the highest, common pixel resolution (0.3mm/pixel).

2.5.2 DEMs of Difference

210 DEMs were exported in ArcMap, and a polygon shapefile was drawn over the area of interest for each block. The
area of interest i.e. the erosion area of the simulated platform surface, was extracted for analysis using the Extract
by Mask' tool in Spatial Analyst tools. DoDs were generated using the Raster was Math tool (minus) in ArcMap
(version 10.5) using Eq. (1),



215
$$B1 DoD_1 = B1 DEM_1 - B1 DEM_0 \quad (1)$$

where the subscript refers to the experimental stage.

2.5.3 Rugosity

220 To permit evaluation of the impact of different degrees of surface roughness on the accuracy and reliability of our generated DEMs, a rugosity index for each block was calculated in ArcMap using the standard Surface Area ratio method (Dahl, 1973; Risk, 1972) where,

$$Rugosity = \frac{Contoured\ area}{Planar\ area} \quad (2)$$

225 A rugosity index (RI) of 1 indicates a planar surface while increasingly higher values indicate increasingly 'rougher' surfaces. The contoured area for each block was calculated using the relevant baseline DEM. A TIN surface was generated using the Raster to TIN tool in ArcMap. The contoured surface area for the specified region was calculated using the Polygon Volume tool in ArcMap. The planar surface area of the same region was derived using the calculate geometry tool assuming negligible change in slope over the specified area. The RI was calculated using Eq. (2).

230

2.5.4 DEM accuracy and error propagation

235 The coded and non-coded markers fixed to the table were used as checkpoints to determine the horizontal (XY) error of the DEMs produced using the CRS (Verma and Bourke). For each DEM, the model and its respective orthophoto were imported into ArcMap (version 10.5) and the distance between 30 randomly selected checkpoints and the two coded scale bars (Figure 1) were measured using the measurement tool. The horizontal error was calculated as the Root Mean Square Error (RMSE) of the difference between measured length and known length.

240 To determine the vertical accuracy of the DEMs, eight wooden blocks were used as checkpoints (Figure 1). The DEMs and orthophotos were imported in ArcMap where the height of wooden blocks were measured using the Interpolate Line tool, by drawing a line across one of the sides of the wooden block and extending it to the ground surface. We ensured that the line drawn was straight. Height was estimated as the difference in mean elevation between wooden block top surface and the surrounding ground surface on each side. The actual height of wooden blocks was measured by an electronic digital Vernier Caliper. The Vernier Caliper has an accuracy of 0.03 mm and measurement repeatability of 0.01 mm. We obtained five measurements along the same side of wooden block measured in ArcMap. We used the mean of these five measurements to calculate the height of the wooden block.

245 The actual height was subtracted from the estimated DEM height to calculate the vertical error.

The calculation of a DoD can result in propagation of error associated with the DEMs used in the computation process. As such, an error analysis is required to increase confidence in the DoD results. This is particularly



important when the scale of geomorphic change being detected is of similar magnitude to uncertainties of the DEMs used in the DoD calculation.

250 We determined the minimum level of detection as the most suitable method of error analysis for this study as the development of shore platforms is primarily an erosional process and as such, the spatial coherence of erosion and deposition (Wheaton et al., 2010) is unsuitable as a method for error analysis in this study. Additionally, while probabilistic approaches produce reliable estimates of morphological change (e.g. Brasington et al., 2003; Brasington et al., 2000; Lane et al., 2003), small changes in elevation, such as those measured in this experiment, 255 may be disguised as noise (Williams, 2012). The minimum Level of Detection (LoD) uses the quadratic composition of errors in the original DEMs to estimate the propagated error of the calculated DoD (Brasington et al., 2003; Gómez-Gutiérrez et al., 2014; Lane et al., 2003; Wheaton et al., 2010; Williams, 2012):

$$E_{DoD_i} = \sqrt{(E_{DEM_i}^2 + E_{DEM_i}^2)} \quad (3)$$

Where E_{DoD_i} refers to the LoD calculated as the square root of the combined squared errors of the DEMs used to 260 generate the DoD. If values of E_{DEM_i} and E_{DEM_i} are known, this method can be applied at a global or local scale where the spatial variability of the error terms are known (Lane et al., 2003). We applied Eq. (3) to determine the minimum threshold of detection for each DEM (Williams, 2012) for each stage of the experiment. Changes detected that fall within the limits of detection ($+ LOD_{min}$ or $- LOD_{min}$) calculated using Eq. (1) are considered noise and interpreted as no change.

265

3 Results

3.1 Accuracy and error propagation

DEM generation resulted in a maximum and minimum horizontal (XY) RMSE of 0.23 mm and 0.03 mm respectively. Maximum vertical (Z) RMSE was 0.52 mm with a minimum of 0.23 mm. The minimum limit of 270 detection was calculated at 0 ± 0.27 mm while the maximum LoD was 0 ± 0.71 mm.

Table 1. The horizontal (XY) and vertical (Z) RMSE error for the control block (B-con) and the experimental blocks B1, B2 and B3. LoD for each DoD is also shown.

| DEM | XY RMSE (mm) | Z RMSE (mm) | LoD (0 ± mm) |
|--------------|-----------------|----------------|-----------------|
| B-con | | | |
| 1 | 0.03 | 0.45 | N/A |
| 2 | 0.12 | 0.23 | 0.27 |
| B1 | | | |
| Stage 0 | 0.23 | 0.37 | N/A |
| Stage 1 | 0.12 | 0.39 | 0.54 |
| Stage 2 | 0.22 | 0.44 | 0.56 |

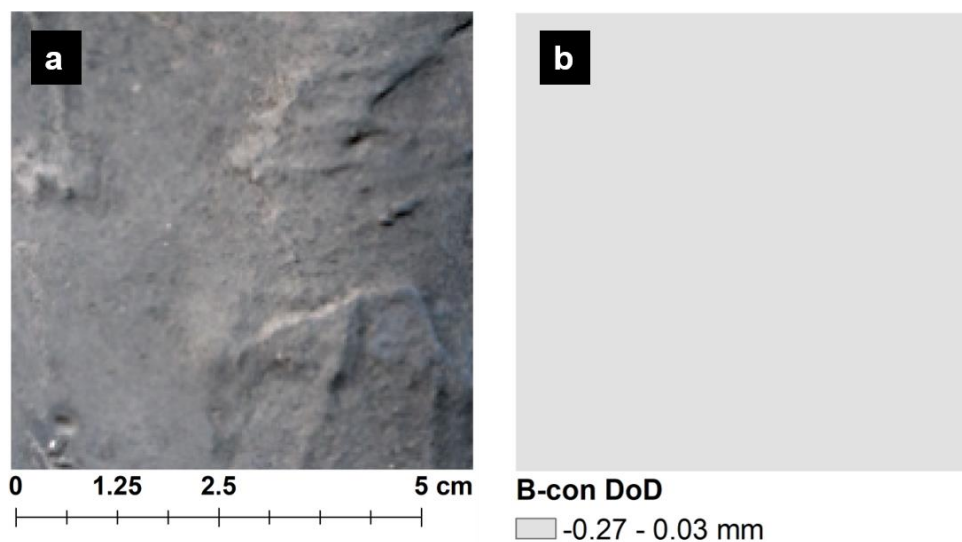


| | | | |
|-----------|------|------|------|
| Stage 3 | 0.12 | 0.52 | 0.71 |
| B2 | | | |
| Stage 0 | 0.1 | 0.40 | N/A |
| Stage 1 | 0.2 | 0.46 | 0.53 |
| Stage 2 | 0.1 | 0.35 | 0.49 |
| Stage 3 | 0.2 | 0.45 | 0.56 |
| B2 | | | |
| Stage 0 | 0.2 | 0.39 | N/A |
| Stage 1 | 0.1 | 0.37 | 0.54 |
| Stage 2 | 0.1 | 0.39 | 0.54 |
| Stage 3 | 0.1 | 0.45 | 0.60 |

275

3.2 Repeatability

The change in vertical elevation for the control block calculated from the DoD is shown in Figure 2 below. The maximum change in elevation (- 0.29 mm) is within the LoD and is interpreted as no change.



280 **Figure 2.** (a) The control block (B-Con) orthophoto and (b) DoD showing a change in surface elevation between successive DEMs.



3.3 Rugosity

285 The RI calculated for each block is shown in Table 2. The control block (B-con) had the lowest rugosity (planar surface) while B1 had a very low RI followed by B2 and B3 in order of increasing rugosity.

Table 2. Contoured surface area (SA), planar surface area and Rugosity Index (RI) for each of the experimental blocks.

| Block ID | Contoured SA (mm) | Planar SA (mm) | R Index |
|----------|----------------------|-------------------|---------|
| B-con | 8.9 | 8.9 | 1.00 |
| B1 | 9.0 | 8.9 | 1.01 |
| B2 | 11.7 | 10.9 | 1.07 |
| B3 | 9.9 | 8.2 | 1.21 |

290 3.3.1 Very low rugosity platform: B1

The results for experimental block B1 are shown in Figure 3 (a-i). The surface area of B1 used in the analysis is shown in (a) where light grey indicates the area of abrasion. For B1 Abrasion, a maximum negative surface change of 1.06 mm was detected, while an increase of 0.30 mm was observed (b) before the LoD was applied. The area of negative surface change between 0.1 mm and 1.06 mm corresponds to the actual area abraded. After thresholding at the LoD, the area of change detected is significantly lower (less than half) the area where the actual change occurred. No increase in surface elevation was detected. For B1 Scratches, the scratched surface is shown in d (black arrows). Before thresholding, the maximum negative change on the surface of B2 was 0.35 mm while an increase in surface elevation of 0.26 mm was detected. Negative changes corresponded well to the observed locations of scratches. After thresholding at the LoD, no changes were detected on the block surface (f). For B1 impact percussions, the locations where block fragments were removed are shown in G (black arrows). Maximum negative change detected, i.e. predicted depth of percussions, was 1.49 mm, while a positive change in surface elevation of 0.30 mm was detected before thresholding (H). After thresholding, no positive change in surface elevation was detected and predicted negative change corresponded well to the actual location of percussions (i).

305 To summarise, for a simulated platform with a very low RI, sweeping abrasion and chips were reliably detected in the thresholded DoD. Scratch depths were less than the LoD and as such were not detected in the thresholded model.

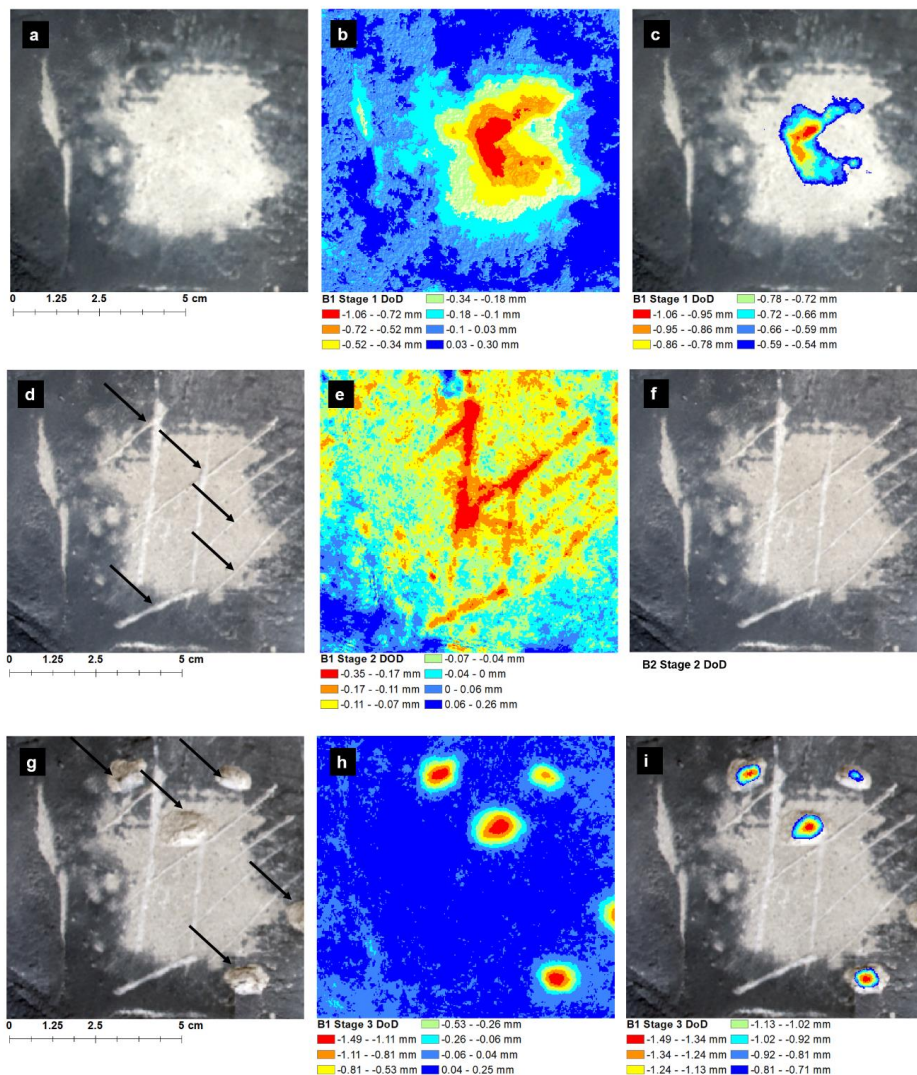


Figure 3. (a) B1 Stage 1 Orthophoto showing abraded surface of simulated platform surface (light grey). (b) DoD for B1 Stage 1 before thresholding at LoD and the thresholded DoD (c). (d) B1 Stage 2 orthophoto showing location of scratches, (e) B1 Stage 2 DoD before thresholding and (f) DoD shown in E thresholded at LoD. (g) B1 Stage 3 orthophoto showing locations of percussions. (h) B1 Stage 3 DoD before thresholding at the LoD and the thresholded DoD (I).



3.3.2 Moderate rugosity platform (B2)

315 The results for experimental block B2 are shown in Figure 4 (a-i). Abraded surface area is indicated by lighter
tone areas in Figure 4a. While this abrasion is visible in the DOD (Figure 4b), a significant component of the
detected change occurred where no change was expected. This corresponds to 'shadow zones' associated with
topographic highs. This result was not affected by thresholding at the LoD (Fig. 4c).

Scratches are evident in Figure d. Furthermore, the location of negative change corresponds well to the location
320 of scratches (Fig. 4e). However, similar to B1, a small area of change is detected around the deepest scratch where
none is expected (Fig. 4f). The impact percussion features are shown in (Fig. 4g). The maximum negative change
in the surface elevation detected (i.e. the depth of percussions), was 3.35 mm, while the maximum positive change
was 0.57 mm (h). Following thresholding, no positive change in elevation was detected (Fig. 4i) and negative
change corresponded well to the actual location of percussions.

325

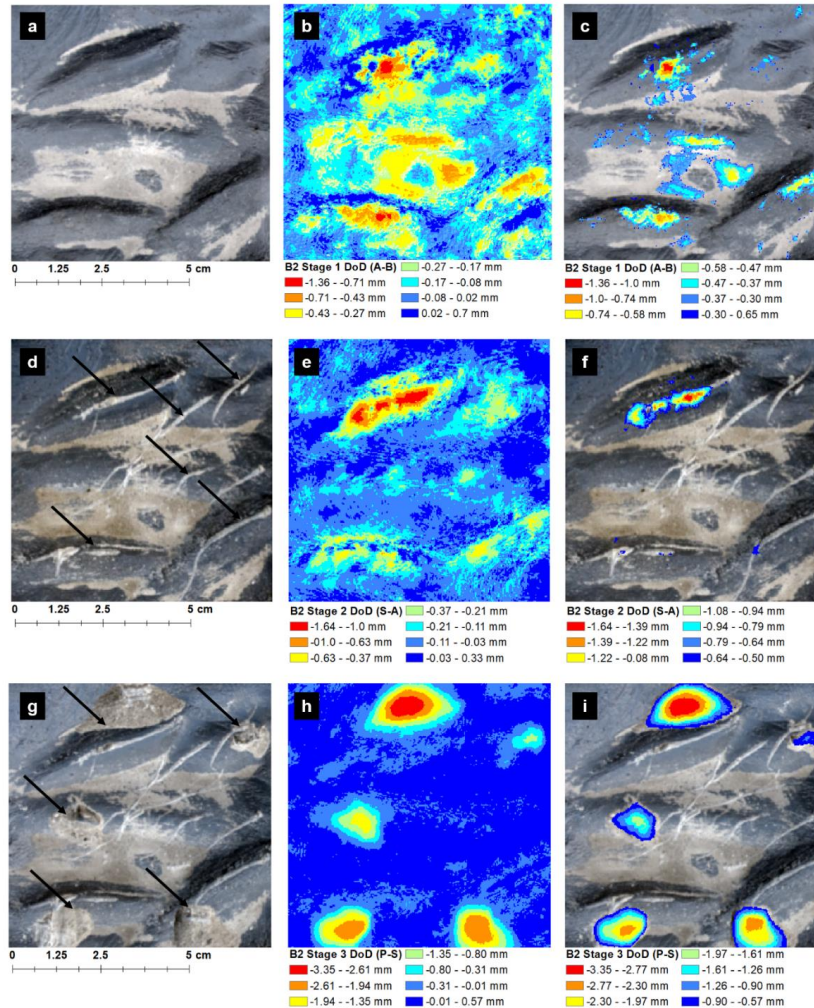


Figure 4. (A) B2 Stage 1 Orthophoto showing abraded area (light grey) of simulated platform surface, (B) B2 Stage 1 DoD before thresholding at LoD and the thresholded

DoD (C). (D) B2 Stage 2 orthophoto showing scratched surface of B2 (black arrows). (E) B2 Stage 2 DoD before thresholding and (F) DoD shown in E thresholded at LoD. Note change detected in shadow zones in F (white arrow) where none is expected. (G) B2 Stage 3 orthophoto percussed surface. (H) DoD before thresholding at LoD and (I) DoD thresholded using calculated LoD.

To summarise, for a simulated platform with a moderate RI, only scratches and impacts were detected in the thresholded DoD.

335



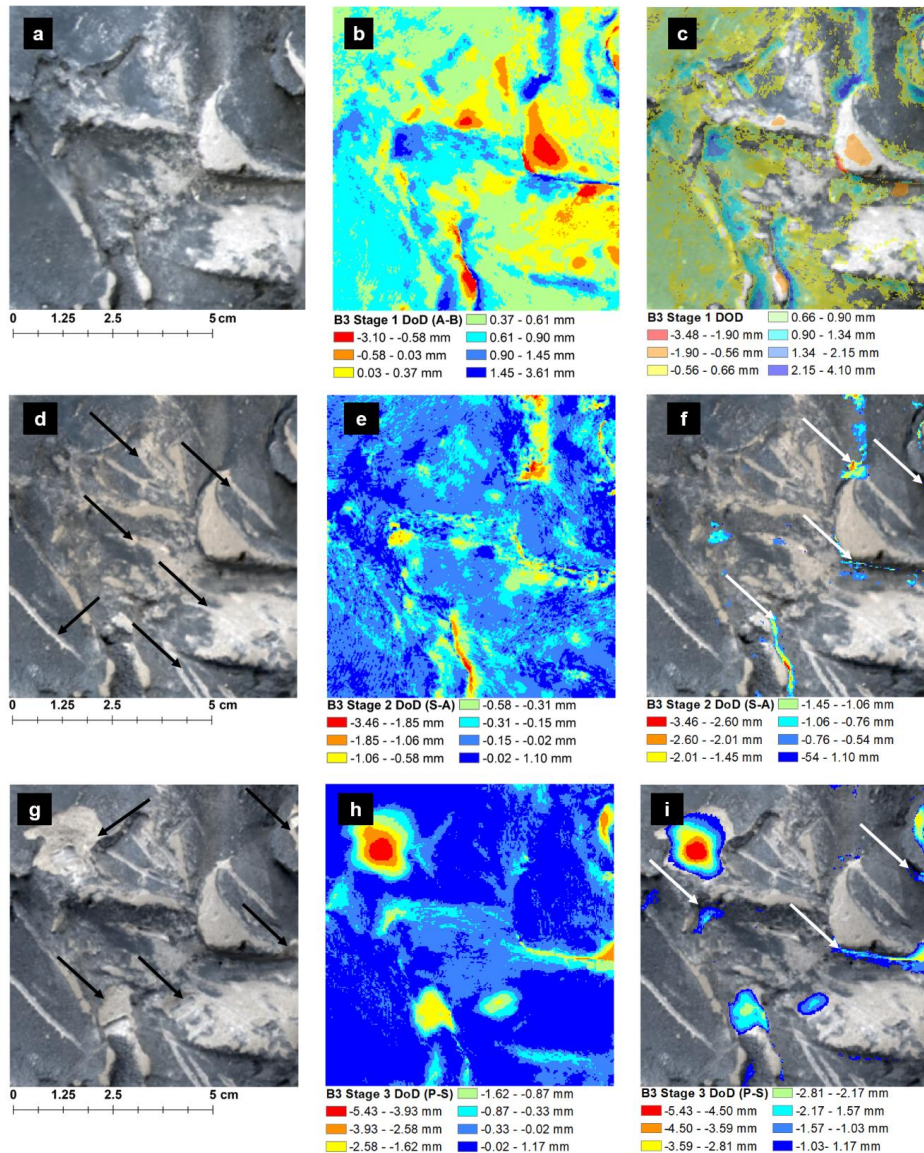
3.2.3 Relatively high rugosity platform (B3)

The results for B3 are shown in Figure 5 (a-i). The light toned areas in (a) indicate the abraded surface of the experimental block. In general, the maximum negative change detected (red and orange areas in b) correspond well to the abraded area. However there are significant increases and decreases (>3 mm) in surface elevation where no change was expected. As above, the largest of these errors generally occurred in ‘shadow zones’.

340 Thresholding did not significantly improve the resultant DoD (i). For scratches (Fig. 5d) there was a reduction in surface elevation of 3.45 mm detected where no change was expected. As with the previous stage, these changes were observed to occur in shadow zones. Thresholding at the LoD did not improve the resultant DoD, and both increases and decreases were recorded where no change was expected (white arrows in i). The location percussions are shown in Figure 5g. Maximum negative change detected corresponded mainly to the location of percussion

345 however negative change was recorded where none was expected (h). As before, abnormal change occurred in shadow zones. Thresholding improved the resultant DoD (i), and the majority of negative change observed corresponded well to the location of percussions, except in some small areas (white arrows in i), associated with shadow zones. Maximum percussion depth was recorded at 5.43 mm.

350 To summarise, for a simulated platform with a relatively high RI, only impacts were reliably detected in the thresholded DoD. However there were errors (larger than in B2) in the data, which are concentrated in topographic ‘shadows’.



355 **Figure 5.** (A) B3 Stage 1 Orthophoto showing abraded surface area (light grey) of simulated platform surface.
 (B) DoD for B3 Stage 3 before thresholding and (C) DoD at LoD shown at 50% transparency overlay onto the
 orthophoto shown in A. Note significant geomorphic change detected in shadow zones (white arrows) where no
 change is expected. (D) B3 Stage 2 orthophoto showing scratched the surface of the simulated platform (black
 arrows), (E) DoD before thresholding and (F) DoD thresholded at LoD. As in C, note change higher than the LoD
 360 detected in shadow zones (white arrows) in F where no change is expected. (G) B3 Stage 3 orthophoto showing



the location of percussions (black arrows), (H) B3 Stage 3 DoD before thresholding at LoD and (I) B3 Stage 3 DoD thresholded using calculated LoD. Note shadow zones (white arrows) where DoD indicates change, but none is expected.

365 3.3 Comparison of the T/MEM and SfM-MVS for measuring erosion on rock shore platforms

The T/MEM has, over decades, cemented its position as a low-cost method for measuring microscale erosion on shore platforms, while SfM-MVS is fast emerging as a valuable tool in the geomorphologists toolkit for the detection and measurement of geomorphic change at a range of scales. Both approaches have advantages and limitations and the choice for use one method over another will depend on a number of factors such as cost, the ease of data collection and the quality and value of the data obtained.

We have compared our experience of using the T/MEM to that of the SfM-MVS (based on the CRS and workflow used in this study) as a means for detecting geomorphic change on rock shore platforms under the following headings. We evaluated both techniques for; ease of data acquisition (including both installation and data collection), data processing, hardware costs, software costs, model resolution, accuracy and overall ease of use. Our reported installation, data collection and data processing times refer to a single measurement station. Hardware costs for the T/MEM are based on initial outlay for SDS drill, drill bits, the T/MEM platform and engineers gauge. Hardware for the SfM-MVS workflow described in this study refers to initial outlay for the manufacture of CRS and cost of the camera. Basic hardware costs (e.g. computer for processing) are not included. Overall ease of use for each method is based on our experience of data acquisition in the field (installation and collection) and data processing. An overall comparison is provided based on the above factors in addition to the value of the data obtained.

A comparison of the T/MEM and the SfM-MVS approach as a means for detecting geomorphic change on rock shore platforms is shown in Figure 6. Both methods have clear advantages and disadvantages and the comparison is intended to be a guide to assist researchers in choosing the most appropriate method for specific project deliverables.

3.3.1 Installation

To install a single T/MEM measurement station, three holes are drilled at the apex of an equilateral triangle and pins set into each hole with a marine grade epoxy resin. The time needed to install a single T/MEM station varies between 40 and 80 minutes depending on rock hardness. For the workflow used in this study, the time needed to install a single bolt to mount the CRS will take approximately one-third of the time.

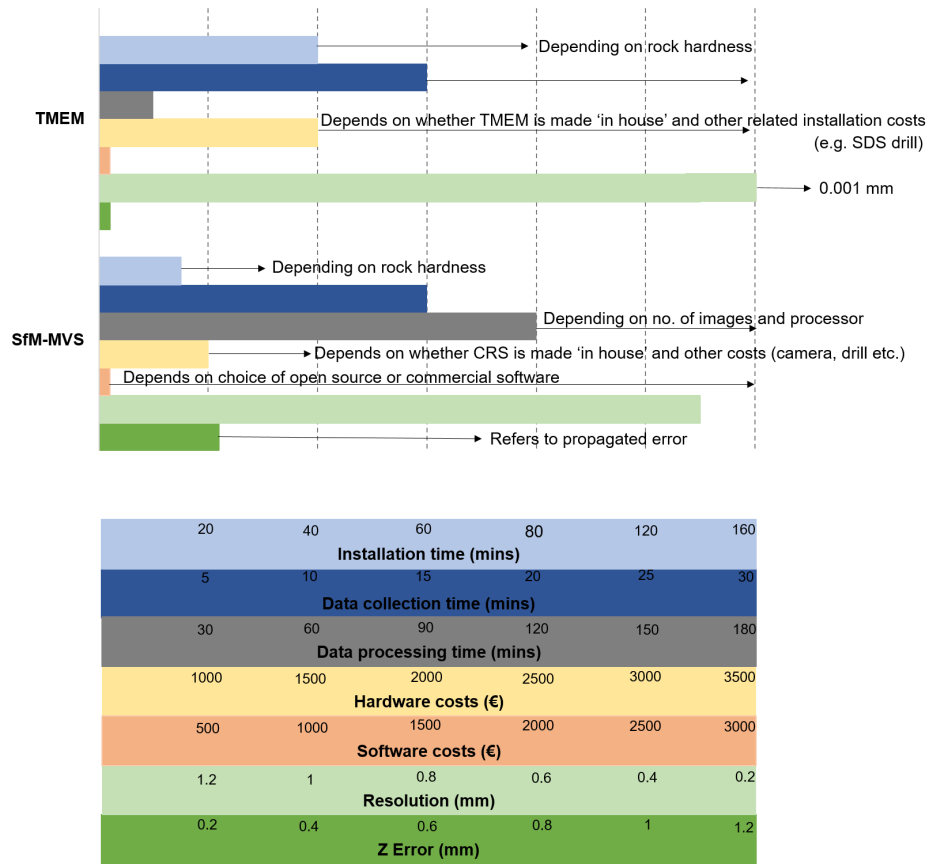


Figure 6. Comparison of TMEM and the SfM – MVS workflow presented in this study under different categories. Values showed (cost, time etc) increase from left to right apart from ‘Resolution’ where decreasing values from left to right indicate increasing resolution.

395

3.3.2 Data collection

In our experience, the time needed to collect data from a single station (based on 100 measurements) using a TMEM varies between 15-30 mins (grey bar in figure 6). This will depend on whether the digital gauge being used has a USB memory, which automatically stores measurements as they are taken (e.g. Stephenson, 1997), or whether measurements are recorded manually which increases the time required. In comparison, acquiring the 40-50 images required for SfM-MVS took approximately 15 minutes.



3.3.3 Data processing

The time required to process TMEM data will depend on the number of measurements collected and the method used to record data in the field, i.e. whether they are stored automatically (e.g. Stephenson, 1997) or manually. Automatic recording reduces the time needed to process data however manual processing can take up to 30 minutes per station (based on 100 measurements). Data processing takes significantly longer for SfM-MVS (2-3 hours per DEM) depending on number of images and the processor used.

3.3.4 Hardware costs

The cost of a TMEM platform varies considerably depending on whether it is made in-house or commercially. In-house construction is considerably less (~€900 for materials and labour), while a commercial TMEM costs approximately €2000 (based on 2017 prices). The cost of the digital gauge also varies depending on the manufacturer, model, resolution, accuracy and Ingress Protection (IP) needed and range from €200-€500. Most rock types will also require an SDS drill with masonry bits which cost in the region of €600. The cost of the 316 stainless steel pins also varies depending on whether they are constructed 'in-house' or purchased commercially.

3.3.5 Software costs

Software cost for TMEM data processing is negligible while there are free open source software available for processing of images for SfM-MVS (e.g. VisualSfM). However, commercial packages such as Agisoft Photoscan can cost between €600 and €3500 depending on the licence type (e.g. Pro, Standard, Educational, Stand alone or Floating).

3.3.6 Resolution and Error

Depending on the digital gauge used, TMEM measurements can have a resolution of up to 0.001 mm with a reported measurement error of ± 0.005 mm (Gómez-Pujol et al., 2007). Resolution for SfM-MVS (achieved in this study) was 0.3 mm per pixel. For some DEMs it was less than this (0.15 mm per pixel) however differencing of DEMs requires that pixel resolution be the same for both DEMs being compared. The CRS and SfM-MVS workflow employed for this study achieved maximum XY and Z RMSE errors of 0.2 mm and 0.5 mm respectively.

4 Discussion

The T/MEM has contributed significantly to our understanding of microscale erosion processes on shore platforms. Measurements of microscale platform erosion using a T/MEM are limited to repeated point measurements over time which provide a mean rate of surface downwearing within the measurement area for that measurement period with the dominant process(es) being inferred from the spatial and temporal variation in downwearing rates (Trenhaile, 2003). However, the method's inability to measure erosion at different scales was noted by Stephenson and Finlayson (2009) as a limitation and the authors advocated the introduction of new



440 methods for measuring shore platform erosion at a range of scales. We have developed a CRS which can be quickly deployed by researchers in the field for detection of micro and meso-scale erosion on shore platforms using SfM-MVS Photogrammetry and a geomorphic change detection approach. The CRS described in this study permits rigorous georeferencing of DEMs derived using the SfM-MVS workflow.

445 We have demonstrated that SfM-MVS Photogrammetry can be used to reliably detect sub-mm changes on shore platforms where the platform surface has a low RI. This approach successfully detected 0.3 mm downwearing of the simulated platform surface of B1 caused by abrasion of the surface. While we were also able to identify shallow scratches on surface of the experimental block, applying the LoD obscured this finding due to the shallow depth of scratches (< 0.3 mm). However, we were able to detect loss of mm-cm sized rock effectively. This demonstrates that our approach offers a method for cross scalar analysis of erosion on shore platforms, offering a much-needed means to examine relationships between micro and meso-scale processes of shore platform erosion and morphologies.

450 Our results indicate that as RI increases, the reliability of SfM-MVS for detection fine scale erosion is reduced due to increased topographic complexity. Despite areas of reduced elevation, i.e. erosion, aligning well with areas where the surface had been abraded, there were areas of change where clearly none was expected. Despite this, our approach successfully detected the loss of rock fragments on the simulated platform surface of B2 (higher RI) once the LoD was applied. Similarly, for B3, which had the highest RI, fine-scale erosion and scratches were not detected reliably, and while the loss of rock fragments was detected, the effect of complex topography in creating shadows zones produced abnormal change. The orthophotos were important in this regard as they provided visual validation of the models and highlighted the influence of shadow zones in introducing error into the models. The additional uncertainty introduced into the models due to the surface complexity was not accounted for using the LoD approach. This resulted in abnormal change detection associated with meso scale (> 1mm) slopes and troughs. While the strong influence of surface complexity may be considered a limitation, it should be noted that
460 the T/MEM is largely restricted to measurements of downwearing on small surface areas with low topographic complexity. As such, it does not exclude this approach as an alternative for measuring change on this type of surface.

465 Precision mapping (James et al., 2017) offers a potential approach to address this as there is an opportunity to increase confidence in the accuracy of point clouds derived for more complex platform morphologies. While the LoD assumes a global uniform distribution of error, precision mapping explicitly accounts for the spatially variable precision characteristic of photo-based surveys (James et al., 2017) and has been demonstrated to improve change detection in areas with complex topography. Future work will test this approach.

470 This study and our experience in the field using a TMEM suggest that the time required for data collection (installation and acquisition) collection is shorter using an SfM-MVS approach compared to the TMEM. The requirement of just one bolt per measurement site for the CRS described here, compared to three bolts per measurement site for the TMEM, reduces the time needed for initial installation in the field. Add to that the time required to collect images for the SfM-MVS workflow compared to the time required to collect 100 TMEM measurements, and SfM-MVS has notable advantages. This reduced installation and data acquisition time are of particular worth for shore platforms with meso to macro tidal ranges, where time in the intertidal zone is limited



475 to, at most, a couple of hours either side of low tide. For larger platforms, where a number of measurement stations
are located in the intertidal zone, time is clearly a limiting factor, and methods which allow rapid installation data
collection are preferable. Regarding data processing, the time required depends on the gauge used to collect the
TMEM data, i.e. manual or automatic and the desired output (point measurements or 3D surface). Regardless,
the processing time required for SfM-MVS is significantly higher (2-3 hours per DEM generated). Nevertheless,
480 batch processing options in Photoscan mean that DEM generation process/steps can be automated and the user
time on computer is reduced. With respect to image acquisition for SfM-MVS, we used a Nikon D5500 and had
included this in our overall analysis however expensive cameras are not a prerequisite. For example, in a recent
experimental study of surface features in sand caused by sublimation of CO₂ ice, of a similar scale to this study,
Mc Keown et al. (2017) used an iPhone to acquire images and utilised the same CRS developed in Verma and
485 Bourke (to scale and reference DEMs, achieving similar accuracy and resolution (<1 mm).

The T/MEM offers considerable resolution and accuracy for measurements of very small surface changes, which
is particularly useful for measuring very slow rates of downwearing and detection of very small changes due to
platform swelling (e.g. Gómez-Pujol et al., 2007; Hemmingsen et al., 2007; Porter and Trenhaile, 2007;
Stephenson and Kirk, 2001; Trenhaile, 2006). For faster-eroding rocks, the precision obtainable using a T/MEM
490 is not required (Stephenson and Finlayson, 2009). While the highest common resolution of the DEMs produced
for this study were 0.3 mm/pixel, this is demonstrated to be sufficient for measuring micro-scale and meso scale
erosion on surfaces with low RI and loss of rock fragments on more topographically complex surfaces.

In terms of data output, the TMEM produces a series of surface point measurements. These can be compared
directly to point measurements made from previous surveys or plotted as a digital elevation model for 3D
495 visualisation of the surface at the bolt site (e.g. Stephenson, 1997). The spatial and temporal variation in
downwearing rates can be used to infer the efficacy of erosion processes. In this, we suggest that SfM-MVS has
a clear and important geomorphic advantage. The technique produces point clouds and DEMs which can be used
to identify and classify surface features as well as detect geomorphic change at different scales. This added value
in the approach is significant. Orthophotograph mosaics offer additional means for validating meso scale changes
500 on the rock surface and identifying erosion styles.

5 Conclusions

1. This study demonstrates that SfM can be used to detect sub-mm changes due to erosion on shore platforms.
However, we find that as the complexity of the rock surface topography increases, the reliability of SfM to detect
505 sub-mm changes decreases. We note that the application of TMEM is also limited to relatively planar surfaces.
Future work will test the precision mapping approach of James et al. (2017) to determine spatial distribution of
error and increase confidence in results on more topographically complex platform surfaces.

2. While TMEM has higher resolution and accuracy compared to SfM, it offers a limited number of point
measurements over a small area. In comparison, SfM produces 3D topographic data from dense point clouds and
510 DEMs which can be used to identify, classify and quantify different styles and scales of erosion.



3. In this study, we have provided a detailed comparison between TMEM and SfM methods to measure change due to erosion on rock surfaces in the coastal environment.

Data availability

515 All data is available upon request from the corresponding author at cullenni@tcd.ie

Author contributions

N.D.C. prepared and wrote the main body of the manuscript with discussion and contributions from A.K.V. and M.C.B. N.D.C. designed the experiment with input from A.K.V. and M.C.B. A.K.V. designed the original
520 coordinate reference system and N.D.C designed the field adapted version with input from A.K.V and M.C.B. N.D.C and A.K.V carried out the experiments. A.K.V. processed images and generated the digital elevation models. N.D.C. carried out data analysis. A.K.V. and M.C.B reviewed and edited the final manuscript.

Acknowledgements

525 N.D.C and A.K.V were supported by the Trinity College Dublin Postgraduate Studentship, Faculty of Engineering, Mathematics and Science. The authors would also like to thank the Geography Department at Trinity College Dublin for additional support in carrying out this research. Our thanks also to Neil Dawson from J.F. Dunne Engineering for expertise in the manufacture of the field adapted coordinate reference system used in the experiment.

530

References

- Balaguer-Puig, M., Marqués-Mateu, Á., Lerma, J. L., and Ibáñez-Asensio, S.: Estimation of small-scale soil erosion in laboratory experiments with Structure from Motion photogrammetry, *Geomorphology*, 2017. 2017.
- Bourke, M. C., Brearley, J. A., Haas, R., and Viles, H. A.: A photographic atlas of rock breakdown features in
535 geomorphic environments, 2007. 2007.
- Brasington, J., Langham, J., and Rumsby, B.: Methodological sensitivity of morphometric estimates of coarse fluvial sediment transport, *Geomorphology*, 53, 299-316, 2003.



- Brasington, J., Rumsby, B., and McVey, R.: Monitoring and modelling morphological change in a braided gravel-bed river using high resolution GPS-based survey, *Earth Surface Processes and Landforms*, 25, 973-990, 540 2000.
- Brunier, G., Fleury, J., Anthony, E. J., Gardel, A., and Dussouillez, P.: Close-range airborne Structure-from-Motion Photogrammetry for high-resolution beach morphometric surveys: Examples from an embayed rotating beach, *Geomorphology*, 261, 76-88, 2016a.
- Brunier, G., Fleury, J., Anthony, E. J., Pothin, V., Vella, C., Dussouillez, P., Gardel, A., and Michaud, E.: 545 Structure-from-Motion photogrammetry for high-resolution coastal and fluvial geomorphic surveys, *Géomorphologie: relief, processus, environnement*, 22, 147-161, 2016b.
- Carbonneau, P. E., Lane, S. N., and Bergeron, N. E.: Catchment-scale mapping of surface grain size in gravel bed rivers using airborne digital imagery, *Water resources research*, 40, 2004.
- Carrivick, J. L., Smith, M. W., and Quincey, D. J.: Structure from Motion in the Geosciences, John Wiley & 550 Sons, 2016.
- Chandler, J.: Effective application of automated digital photogrammetry for geomorphological research, *Earth Surface Processes and Landforms*, 24, 51-63, 1999.
- Chandler, J., Ashmore, P., Paola, C., Gooch, M., and Varkaris, F.: Monitoring river-channel change using terrestrial oblique digital imagery and automated digital photogrammetry, *Annals of the Association of 555 American Geographers*, 92, 631-644, 2002.
- Dahl, A. L.: Surface area in ecological analysis: quantification of benthic coral-reef algae, *Marine Biology*, 23, 239-249, 1973.
- Fonstad, M. A., Dietrich, J. T., Courville, B. C., Jensen, J. L., and Carbonneau, P. E.: Topographic structure from motion: a new development in photogrammetric measurement, *Earth Surface Processes and Landforms*, 560 38, 421-430, 2013.
- Furukawa, Y., Curless, B., Seitz, S. M., and Szeliski, R.: Towards internet-scale multi-view stereo, 2010, 1434-1441.
- Gómez-Gutiérrez, Á., Schnabel, S., Berenguer-Sempere, F., Lavado-Contador, F., and Rubio-Delgado, J.: Using 3D photo-reconstruction methods to estimate gully headcut erosion, *Catena*, 120, 91-101, 2014.
- 565 Gómez-Pujol, L., Stephenson, W. J., and Fornós, J. J.: Two-hourly surface change on supra-tidal rock (Marengo, Victoria, Australia), *Earth Surface Processes and Landforms*, 32, 1-12, 2007.
- Hanna, F.: A technique for measuring the rate of erosion of cave passages, *Proceedings University of Bristol Speleology Society*, 11, 83-86, 1966.



- Hemmingsen, S. A., Eikaas, H. S., and Hemmingsen, M. A.: The influence of seasonal and local weather
570 conditions on rock surface changes on the shore platform at Kaikoura Peninsula, South Island, New Zealand,
Geomorphology, 87, 239-249, 2007.
- James, M. R., Robson, S., and Smith, M. W.: 3-D uncertainty-based topographic change detection with
structure-from-motion photogrammetry: precision maps for ground control and directly georeferenced surveys,
Earth Surface Processes and Landforms, 2017. 2017.
- 575 Javernick, L., Brasington, J., and Caruso, B.: Modeling the topography of shallow braided rivers using
Structure-from-Motion photogrammetry, *Geomorphology*, 213, 166-182, 2014.
- Kaiser, A., Neugirg, F., Rock, G., Müller, C., Haas, F., Ries, J., and Schmidt, J.: Small-scale surface
reconstruction and volume calculation of soil erosion in complex Moroccan gully morphology using structure
from motion, *Remote Sensing*, 6, 7050-7080, 2014.
- 580 Lane, S. N., Westaway, R. M., and Murray Hicks, D.: Estimation of erosion and deposition volumes in a large,
gravel-bed, braided river using synoptic remote sensing, *Earth Surface Processes and Landforms*, 28, 249-271,
2003.
- Lim, M., Rosser, N. J., Allison, R. J., and Petley, D. N.: Erosional processes in the hard rock coastal cliffs at
Staithe, North Yorkshire, *Geomorphology*, 114, 12-21, 2010.
- 585 Lowe, D. G.: Distinctive image features from scale-invariant keypoints, *International journal of computer
vision*, 60, 91-110, 2004.
- Mc Keown, L., Bourke, M., and McElwaine, J.: Experiments On Sublimating Carbon Dioxide Ice And
Implications For Contemporary Surface Processes On Mars, *Scientific reports*, 7, 14181, 2017.
- Micheletti, N., Chandler, J. H., and Lane, S. N.: Investigating the geomorphological potential of freely available
590 and accessible structure-from-motion photogrammetry using a smartphone, *Earth Surface Processes and
Landforms*, 40, 473-486, 2015a.
- Micheletti, N., Chandler, J. H., and Lane, S. N.: Structure from Motion (SfM) Photogrammetry, 2015b. 2015b.
- Moses, C., Robinson, D., and Barlow, J.: Methods for measuring rock surface weathering and erosion: A critical
review, *Earth-Science Reviews*, 135, 141-161, 2014.
- 595 Özyeşil, O., Voroninski, V., Basri, R., and Singer, A.: A survey of structure from motion*, *Acta Numerica*, 26,
305-364, 2017.
- Porter, N. J. and Trenhaile, A.: Short-term rock surface expansion and contraction in the intertidal zone, *Earth
Surface Processes and Landforms*, 32, 1379-1397, 2007.
- Risk, M. J.: Fish diversity on a coral reef in the Virgin Islands, 1972. 1972.



- 600 Smith, M., Carrivick, J., and Quincey, D.: Structure from motion photogrammetry in physical geography, *Progress in Physical Geography*, 40, 247-275, 2016.
- Snaveley, N.: Bundler: SfM for unordered image collections, Domain: <http://phototour.cs.washington.edu/bundler/>.(15.09. 10), 2006. 2006.
- Stephenson, W. and Finlayson, B.: Measuring erosion with the micro-erosion meter—contributions to
605 understanding landform evolution, *Earth-Science Reviews*, 95, 53-62, 2009.
- Stephenson, W., Kirk, R., Hemmingsen, S., and Hemmingsen, M.: Decadal scale micro erosion rates on shore platforms, *Geomorphology*, 114, 22-29, 2010.
- Stephenson, W. and Naylor, L.: Within site geological contingency and its effect on rock coast erosion, *Journal of Coastal Research*, 64, 831-835, 2011.
- 610 Stephenson, W. J.: Improving the traversing micro-erosion meter, *Journal of Coastal Research*, 1997. 236-241, 1997.
- Stephenson, W. J. and Kirk, R. M.: Surface swelling of coastal bedrock on inter-tidal shore platforms, Kaikoura Peninsula, South Island, New Zealand, *Geomorphology*, 41, 5-21, 2001.
- Thoeni, K., Giacomini, A., Murtagh, R., and Kniest, E.: A comparison of multi-view 3D reconstruction of a
615 rock wall using several cameras and a laser scanner, *The International Archives of Photogrammetry, Remote Sensing and Spatial Information Sciences*, 40, 573, 2014.
- Thornbush, M. J.: A site-specific index based on weathering forms visible in Central Oxford, UK, *Geosciences*, 2, 277-297, 2012.
- Trenhaile, A.: Tidal wetting and drying on shore platforms: an experimental study of surface expansion and
620 contraction, *Geomorphology*, 76, 316-331, 2006.
- Trenhaile, A. S.: Modeling shore platforms: present status and future developments, *Elsevier Oceanography Series*, 67, 393-409, 2003.
- Trudgill, S.: Measurement of erosional weight loss of rock tablets, *British Geomorphological Research Group Technical Bulletin*, 17, 13-20, 1975.
- 625 Trudgill, S., High, C., and Hanna, F.: Improvements to the micro-erosion meter, *British Geomorphological Research Group Technical Bulletin*, 29, 3-17, 1981.
- Verma, A. K. and Bourke, M. C.: A Structure from Motion photogrammetry-based method to generate sub-millimetre resolution Digital Elevation Models for investigating rock breakdown features, *Earth Surf. Dynam. Discuss.*, <https://doi.org/10.5194/esurf-2018-53>, in review, 2018. .
- 630 Viles, H. A.: Scale issues in weathering studies, *Geomorphology*, 41, 63-72, 2001.



Walkden, M. and Hall, J.: A predictive mesoscale model of the erosion and profile development of soft rock shores, *Coastal Engineering*, 52, 535-563, 2005.

Warke, P. A. and McKinley, J.: Scale issues in geomorphology, *Geomorphology*, 130, 1-4, 2011.

Westoby, M., Brasington, J., Glasser, N., Hambrey, M., and Reynolds, J.: 'Structure-from-Motion' photogrammetry: A low-cost, effective tool for geoscience applications, *Geomorphology*, 179, 300-314, 2012.

Wheaton, J. M., Brasington, J., Darby, S. E., and Sear, D. A.: Accounting for uncertainty in DEMs from repeat topographic surveys: improved sediment budgets, *Earth Surface Processes and Landforms*, 35, 136-156, 2010.

Williams, R.: DEMs of difference. In: *Geomorphological Techniques*, 2 (3.2), British Society for Geomorphology, London, UK, 2012.